Rectification and Nonlinear Optical Properties of a Langmuir−Blodgett Monolayer of a Pyridinium Dye

Jeffrey W. Baldwin,[†] Ramiya R. Amaresh,[†] Ian R. Peterson,[†,‡] Walter J. Shumate,[†] Michael P. Cava,[†] Mukhtar A. Amiri,[§] Richard Hamilton,[§] Geoffrey J. Ashwell,[§] and Robert M. Metzger*[,†]

Laboratory for Molecular Electronics, Chemistry Department, The University of Alabama, Tuscaloosa, Alabama 35487-0336, Centre for Molecular & Biomolecular Electronics, Department of Natural & Environmental Sciences, University of Coventry, Priory Street, Coventry CV1 5FB, United Kingdom, and The Nanomaterials Group, Cranfield University, Cranfield MK430AL, United Kingdom

Received: February 1, 2002

Rectification was observed across a monolayer of 2,6-di[dibutylamino-phenylvinyl]-1-butylpyridinium iodide, $(Bu_2N\varphi V)_2BuPy^+I^-$, **1** sandwiched between gold electrodes. The current is enhanced at a forward bias above 0.5 to 1.0 V, as electrons flow preferentially from the iodide ions to the pyridinium ring, and is as high as 100 000 electrons molecule^{-1} s^{-1}, with a rectification ratio of up to 90.

Introduction

The Aviram-Ratner proposal[1] of a unimolecular electrical rectifier stimulated many experimental efforts,[2,3] which were finally successful,[4,5] and thoroughly confirmed.[6,7] The original proposal suggested a D-σ-A molecule connecting an electron donor moiety (D) to an electron acceptor moiety (A) through an insulating saturated "sigma" bridge σ[1]; the mechanism of action involves inelastic tunneling through the molecule from its first electronic excited-state D^+-σ-A^- to the less polar ground-state D°-σ-A^0.[2,3] The first confirmed rectifier was, however, a ground-state zwitterion D^+-π-A^-, connected by a twisted π bridge, rather than a σ bridge, and used inelastic tunneling from the lower-polarity excited-state D°-π-A^0 to the higher-polarity ground state.[6,7] We have also observed rectification from LB films of a cationic D-π-A dye with sodium octadecyl sulfate as the counterion, which packs side-by-side with the amphiphilic chromophore.[8]

We present here a new monolayer rectifier of a different type. Macroscopic current−voltage measurements show asymmetry in the DC electrical conductivity, i.e., electrical rectification, through the molecule, 2,6-bis-[2-(4-dibutylamino-phenyl-vinyl]-1-butylpyridinium iodide, $(Bu_2N\varphi V)_2BuPy^+I^-$, **1**)as a mono-

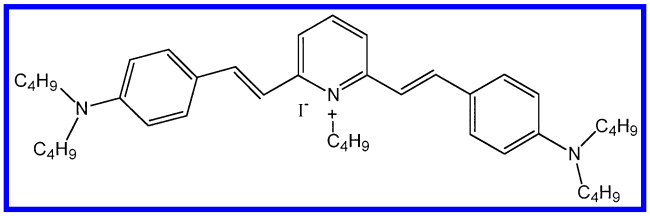

layer between gold electrodes. This molecule and its LB films were characterized by spectroscopic techniques. About two-thirds of the iodide counterions are replaced in the LB film by other counteranions (possibly hydroxide, or bicarbonate). An LB monolayer of $(Bu_2N\varphi V)_2BuPy^+I^-$ also exhibits an effective second-order susceptibility of 150 pm V^{-1} at 45° for $\lambda = 1064$ nm. This new rectifier of electrical current does not function as an Aviram-Ratner molecule. Rather, it functions as an interionic diode, or Schottky barrier diode, whose enhanced electron flow in the forward direction is probably due to the field-induced electron transfer from the iodide anion (or other counteranion) to the pyridinium ring.

The rectification ratios average 4 at ±1.8 V, which corresponds to a field of approximately 900 MV m^{-1} and a current density of 10−1000 mA cm^{-2}, or, using a molecular area of 95 Å^2 (measured by quartz crystal microscopy), 1600−160000 electrons molecule^{-1} s^{-1}.

Synthesis of 1-Butyl-2,6-bis[2-(4-dibutylaminophenyl)vinyl]pyridinium Iodide. A mixture of 2,6-dimethylpyridine (2.14 g, 0.02 mol) and butyl iodide (3.68 g, 0.02 mol) was heated at 130 °C for 18 h, to give a pale yellow solid after cooling and washing with anhydrous ether (38% yield) mp 156−160 °C. ^{1}H NMR ($CDCl_3$, 360 MHz): 8.32 (t, 1H, $J = 7.92$ Hz), 7.91 (d, 2H, $J = 7.92$ Hz), 4.62 (t, 2H, $J = 8.64$ Hz), 3.02 (s, 6H), 1.87 (m, 2H), 1.59 (m, 2H), 1.04 (t, 3H, $J = 7.2$ Hz). The foregoing salt (0.291 g, 0.001 mol) in DMF was treated with piperidine (0.34 g, 0.004 mol), followed by *p*-dimethylaminobenzaldehyde (0.583 g, 0.0025 mol) in 2 mL. The mixture was heated at 120 °C for 34 h. The cooled mixture was diluted with ether, and the red precipitate of the product was filtered, washed with water, and dried (61% yield), mp 203.5−204 °C. ^{1}H NMR ($CDCl_3$, 360 MHz): δ_H 8.20 (t, 1H, $J = 10.81$ Hz), 7.90 (d, 2H, $J = 7.92$ Hz), 7.56 (d, 4H, $J = 7.2$ Hz), 7.48 (d, 2H, $J = 15.48$ Hz), 7.03 (d, 2H, $J = 15.48$ Hz), 6.64 (d, 4H, $J = 7.2$ Hz), 4.75 (t, 2H, $J = 8.64$ Hz), 3.32 (t, 8H, $J = 7.2$ Hz), 1.88 (s, 2H), 1.64 (s, 2H), 1.55 (m, 8H), 1.37 (m, 8H), 1.26 (m, 4H), 1.0384 (t, 3H, $J = 7.2$ Hz), 0.97 (t, 12H, $J = 7.56$ Hz). ^{13}C NMR ($CDCl_3$, 90 MHz): 153.34, 150.28, 143.90, 142.13, 130.68, 122.0, 121.60, 111.56, 110.71, 52.69, 50.8, 30.87, 29.39, 20.25, 17.53, 13.92, 13.81. *m*/*z* (FAB): 594 (100%, $M^+ - I^-$).

* Corresponding author.
† The University of Alabama.
‡ University of Coventry.
§ Cranfield University.

10.1021/jp0203189 CCC: $22.00
Published on Web 11/05/2002

Experimental Details

All measurements, except when specifically noted otherwise, were performed at the University of Alabama. Cyclic voltammograms (CV) were measured in a BAS-100 instrument, in a single-compartment cell with a platinum disk working electrode (1 mm diameter), a platinum wire auxiliary electrode, and a saturated calomel electrode (SCE) as the reference electrode. For each measurement, a 0.1 M solution of tetrabutylammonium hexafluorophosphate in dry solvent was employed with ca. 1 mM of the substrate. The potentials are given at a scan rate of 100 mV/s. A computer-controlled EG&G Potentiostat (PAR263) was used for all the measurements. UV−vis spectra were obtained in a Cary 50 UV−Vis spectrophotometer. Semiempirical theoretical molecular orbital calculations (AM1, PM3) were performed using the CAChe program package (Fujitsu) on a Macintosh G3 microcomputer.

Langmuir−Blodgett (LB) and Pockels-Langmuir (PL) films were studied using a PC-controlled Nima model 622D2 film trough, using 18 MΩ water (Millipore Milli-Q), connected to a constant-temperature bath (12.5 °C), in a temperature-controlled HEPA-filtered room (15.5 °C). The PL monolayer at the air−water interface was studied by Brewster angle microscopy, using a MiniBAM (Nanofilm Technologie, Göttingen, Germany).

The monolayer deposited on 10 MHz crystals was measured at Cranfield in a home-built quartz crystal microbalance (QCM). Its thickness was estimated by spectroscopy ellipsometry (Woolam, Inc.).

The XPS spectrum of a multilayer was measured in a Kratos Axis 165 spectrometer.

The thickness and dielectric permittivities were obtained at Cranfield by analysis of the surface plasmon resonance (SPR) data, obtained from glass|gold|monolayer structures, using p-polarized monochromatic radiation, HeNe or a frequency-doubled Nd:YAG laser, and an attenuated total reflection geometry in the Kretschmann configuration.[9]

Second harmonic generation was measured at Cranfield using a Nd:YAG, p-polarized laser ($\lambda = 1064$ nm).

Macroscopic current−voltage measurements were made on vacuum annealed gold-coated substrates (Corning glass #1747F and Si 100), with a Ti underlayer (50 nm Ti, 100 nm Au) prepared in an Edwards 306A evaporator at 4×10^{-5} mbar. The substrates bearing the fresh Au film were immediately stored under conductivity water, and placed below the Langmuir trough subphase prior to LB deposition. This precaution prevented exposure to atmosphere-born contaminants that would otherwise convert the Au from hydophilic to hydrophobic within 30 min. However, the Au-bearing Si substrate was exposed to trace amounts of water-soluble contaminants that had not been not eliminated in the Millipore deionizing system. The LB monolayer film, deposited on the upstroke (transfer ratio 100%) on the Au-covered glass substrates, was dried in a vacuum desiccator with P_2O_5 for 3 days in the dark, prior to evaporating the top gold electrode. Top gold electrodes were evaporated onto the sample cooled by thermal contact to a coldfinger cooled with liquid nitrogen in an Edwards 306A evaporator, using a "cold gold" technique[10] back-filled with Ar gas at 1×10^{-6} bar. As already described elsewhere,[11] because of the fragile nature of the monolayer, care was taken during the evaporation of the top Au electrode, to avoid damage to the film by thermal radiation or by collision with Au atoms of high-kinetic energy. The top gold electrode, estimated to be 17 nm thick from a similar evaporation,[11] was deposited by back-filling the chamber with Ar to a pressure of 1×10^{-6} bar. The low-energy backscattered Au atoms were evaporated through a contact mask

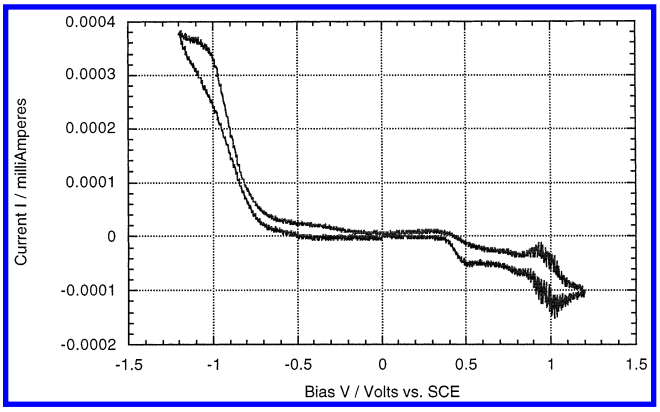

Figure 1. CV of $(Bu_2N\varphi V)_2BuPy^+I^-$ (0.1 M CH_3CN/Bu_4NPF_6, platinum disk working electrode (1 mm diameter), a platinum wire auxiliary electrode, and a saturated calomel reference electrode (SCE), 100 mV/s scan rate) shows reversible oxidation and reduction peaks at $E°_{ox} = 0.52$ V, 1.04 V, and $E°_{red} = -1.08$ V vs SCE.

(0.3 mm^2) at a rate of 0.03 nm min^{-1}. The metal−organic monolayer−metal (MOM) assembly was removed from the vacuum system, and the conductivity of each MOM was characterized, using micromanipulators to make electrical contact, in a shielded Faraday cage. Contact to the gold electrodes was achieved using a Ga/In eutectic (Alfa Aesar, 99.99%) connected to gold wires (Johnson Matthey, 99.998%, 0.05 mm diameter). Current−voltage (*IV*) measurements were obtained using a PC-controlled (Delphi) DC conductivity measuring system, using a HP 3245A universal source, and a HP 3457A multimeter. The rectification ratio (RR) at the applied voltage V_o is defined as

$$RR = [\text{current at } V_o]/[|\text{current}| \text{ at } -V_o]$$

Results

The synthesis can create a mixture of three isomers, the E,E, the E,Z, and the Z,Z isomers. What has been isolated is the E,E isomer.

The CV of $(BuA\varphi)_2-BuPy^+I^-$ (Figure 1) shows two oxidation peaks at $E°_{ox} = 0.52$ V (irreversible), 1.04 V (reversible) vs SCE, and one irreversible reduction peak at $E°_{red} = -1.08$ V vs SCE.

$(Bu_2N\varphi V)_2BuPy^+I^-$ is weakly hypsochromic: its long-wavelength absorption peak is at 519 nm (2.39 eV) in chloroform (dielectric constant $\epsilon = 4.8$) with a molar absorptivity $\alpha = 36\,600$ cm^{-1} M^{-1}; it is at 508 nm (2.42 eV, $\alpha = 52\,000$ cm^{-1} M^{-1}) in acetone ($\epsilon = 20.7$), and at 505 nm (2.46 eV, $\alpha = 45\,000$ cm^{-1} M^{-1}) in acetonitrile ($\epsilon = 39$).

The UV−vis spectra of a small model salt, 1-butyl-2,6-dimethylpyridinium iodide show a much smaller hypsochromic shift, from $\lambda_{max} = 356$ nm in chloroform (dielectric constant $\epsilon = 4.8$), to $\lambda_{max} = 350$ nm in acetone ($\epsilon = 20.7$). It seems clear that both iodides are hypsochromic, with the excited-state dipole moment being smaller than that of the ground state. This may be because the spectroscopic transition is due to an interionic back charge transfer from the iodide to the pyridinium ion in the excited state, as argued decades ago.[12,13]

Theoretical calculations, using CACHe (AM1 and PM3), with methyl groups instead of butyl groups for computational convenience, show (Figure 2) the HOMO at 10.4 eV, with large MO amplitudes mainly on the aniline moiety, and the LUMO at 4.6 eV with significant MO amplitudes mainly on the pyridinium ring.

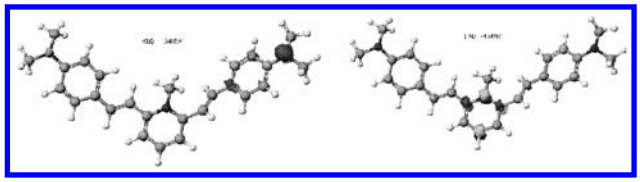

Figure 2. Depiction of significant wave function amplitudes for $(Me_2N\varphi V)_2MePy^+$ using PM3 (AM1 gives similar values) for (left): HOMO, energy $E = 10.4$ eV, and for (right): LUMO energy $E = 4.8$ eV.

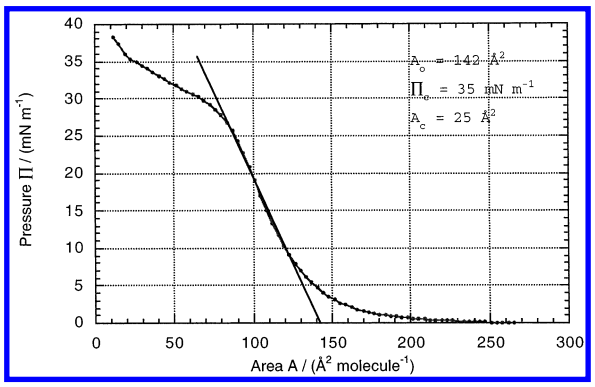

Figure 3. Pressure−area isotherm of $(Bu_2N\varphi V)_2BuPy^+I^-$; subphase $T = 12.5$ °C, barrier speed = 200 cm^2 min^{-1}, pH = 6.5. The molecular areas are $A_o = 142$ Å^2 at zero film pressure, $A_c = 25$ Å^2 at the collapse pressure of 35 mN m^{-1}, and $A_t = 90$ Å^2 at the chosen transfer pressure of 22 mN m^{-1}.

A compact PL monolayer of $(Bu_2N\varphi V)_2BuPy^+I^-$ was formed by spreading a dilute (0.06 mg mL^{-1}) solution in chloroform on the air−water interface, and then decreasing the trough area (200 cm^2 min^{-1}); the pressure−area isotherm is shown in Figure 3. Investigation of the film surface using a Brewster angle microscope shows a uniform film coverage on the air−water interface. The measured areas are $A_o = 142$ Å^2 molecule^{-1} at zero pressure, and $A_c = 25$ Å^2 molecule^{-1} at the inflection point, i.e., at the collapse pressure of 35 mN m^{-1}, and $A_t = 90$ Å^2 at the transfer pressure of 22 mN m^{-1} (see below). It is likely that the more polar pyridinium iodide functional group is closest to the water subphase. The PL monolayer was transferred, on the upstroke at a constant pressure of 22 mN m^{-1} and at a rate of 5 mm min^{-1}, onto a freshly prepared hydrophilic gold-coated substrate, which was submerged in the subphase before spreading and compressing the monolayer.

When the dye is deposited at a surface pressure of 22 mN m^{-1} onto 10 MHz quartz crystals, a Sauerbrey analysis[14] of the frequency change, combined with the measurement of the area covered by the monolayer on the QCM probe, provides an area of 95 ± 5 Å^2 molecule^{-1} in contact with the substrate, compared with only ca. 90 Å^2 (at a transfer pressure of 22 mN m^{-1}) from the pressure−area isotherm. The analysis assumes that the counterion is iodide; and the discrepancy (95 Å^2 vs 90 Å^2) may be explained by anion exchange with OH^- and/or HCO_3^- at the air−water interface: their molar masses are significantly lower than those of iodide, and thus result in an apparent decrease in the contact area obtained from the frequency change. When dissolved in the aqueous subphase, the water-soluble counterion, associated with the dye, has a concentration of ca. 5×10^{-8} mol dm^{-3}, this being significantly less than those of OH^- and HCO_3^-, which occur naturally in the subphase. It is therefore likely that the iodide counterion can be replaced. Alternatively, the larger areas may simply reflect either voids (albeit unlikely, as the data are reproducible) or an altered alignment upon deposition.

Three monolayers were transferred (the first two on the upstroke, the third on a downstroke) on a quartz substrate; their UV−vis spectrum is presented in Figure 4. The molecule shows a maximum absorption maximum at $\lambda_{max} = 490$ nm, which is shifted from the solution spectra by at least 15 nm in the most polar solvent, CH_3CN, and by more than 40 nm when compared to the least polar solvent, $CHCl_3$.

In the X-ray photoelectron spectrum of bulk $(BuA\varphi)_2BuPy^+I^-$ on silicon, after correction for a sensitivity factor, the ratio of the photoelectron signal intensities, for N(1s):I(3d) was 3.21:1.00, while the N:I atom ratio is 3:1. In contrast, in the X-ray photoelectron spectrum of an LB monolayer of $(BuA\varphi)_2BuPy^+I^-$ on Au on silicon, the iodine (3d) signal intensity was much reduced, to one-third the intensity expected from the stoichiometry. In fact, the angle-resolved XPS spectrum intensity ratios SR were [θ, SR = N(1s)/I(3d)] = [0°: SR = 3.29/0.34

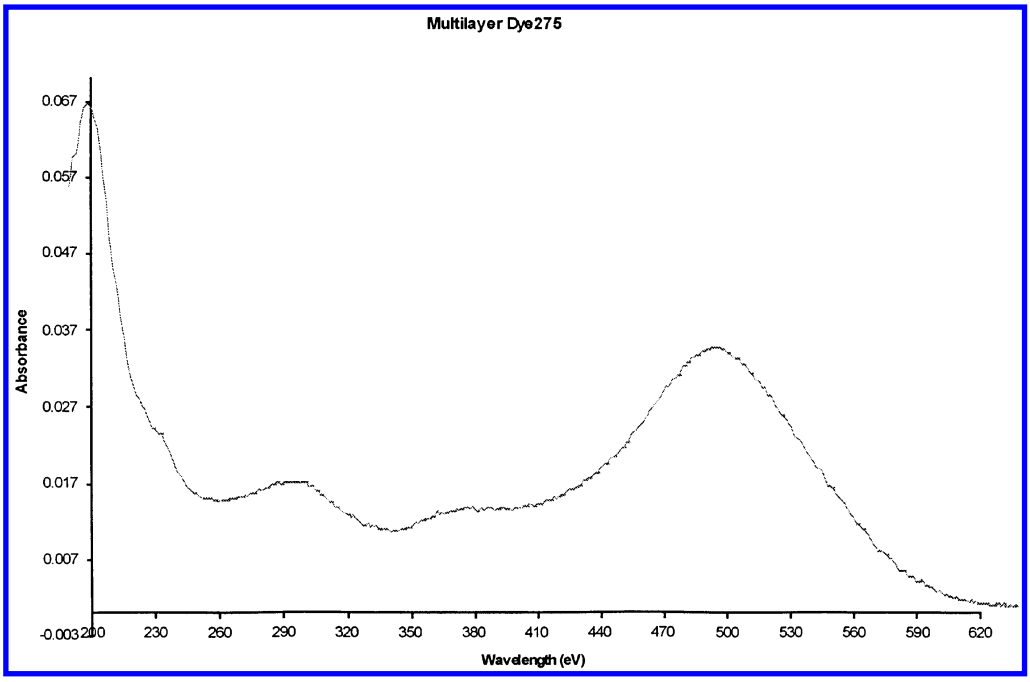

Figure 4. UV−vis spectrum of three monolayers of $(Bu_2N\varphi V)_2BuPy^+I^-$ on glass shows an absorption maximum at 490 nm.

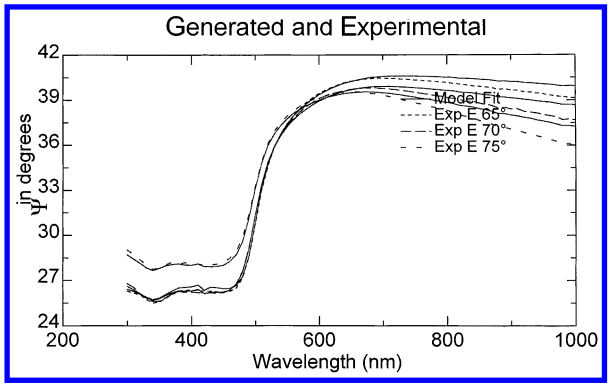

Figure 5. Spectroscopic ellipsometry of monolayer of $(Bu_2N\varphi V)_2$-$BuPy^+I^-$, on "Au|Ti|glass" suggests a film thickness of 0.7 nm, using a Lorentz fit that includes the UV-absorption data of the monolayer.

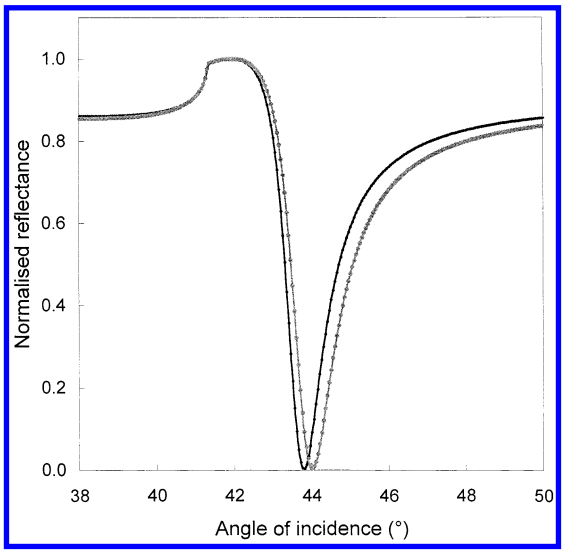

Figure 6. Normalized SPR reflectance from glass/Au and glass/Au/monolayer structures at $\lambda = 632.8$ nm. The thickness and dielectric permittivities of the gold overlay are $l = 47.2$ Å, $\epsilon_r = -11.50$, and $\epsilon_i = 1.27$. Corresponding values for the LB overlay are 11.5 Å, $\epsilon_r = 2.66$, and $\epsilon_i = 0.40$. Almost identical reflectance plots (not shown) are obtained at $\lambda = 532$ nm, for which wavelength, the gold overlay values become $l = 46.5$ Å, $\epsilon_r = -4.62$, and $\epsilon_i = 2.13$, while the LB overlay data become 11.8 Å, $\epsilon_r = 3.12$, and $\epsilon_i = 0.70$.

$= 9.7$; 15°: SR $= 4.35/0.44 = 9.9$; 30°: SR $= 4.35/0.44 = 9.9$; 45°: SR $= 4.79/0.41 = 12$; 60°: SR $= 2.74/0.39 = 7.0$]. Thus, it seems that about two-thirds of the iodide ions may have been replaced by some other anion, as discussed below.

A monolayer of $(Bu_2N\varphi V)_2-BuPy^+I^-$, transferred atop a 50 nm Au film (above a 20 nm Ti adhesion layer on glass), was studied by spectroscopic ellipsometry: the data of Figure 5 suggests that the monolayer thickness is 0.7 nm.

SPR thicknesses, obtained by using HeNe and frequency-doubled Nd:YAG excitatory wavelengths (Figure 6), are 11.5 and 11.8 Å, respectively (cf. 14 Å van der Waals height); these values indicate that the chevron-shaped molecule is tilted very slightly toward the plane of the substrate. The product of thickness and contact area (95 ± 5 Å^2 from QCM data, assuming that iodide is the counterion) gives a volume of 1160 ± 20 Å^3, from which the film density is estimated as 1.03 ± 0.02 g cm^{-3}. In fact, this derived density is independent of the counterion, which may be I^-, OH^-, or HCO_3^-, or any combination.

The real and imaginary components of the dielectric permittivity are $\epsilon_r = 2.66$ and $\epsilon_i = 0.40$ at $\lambda = 632.8$ nm, and $\epsilon_r = 3.12$ and $\epsilon_i = 0.70$ at $\lambda = 532$ nm. The differences are consistent with the visible spectrum, which exhibits a peak absorbance at

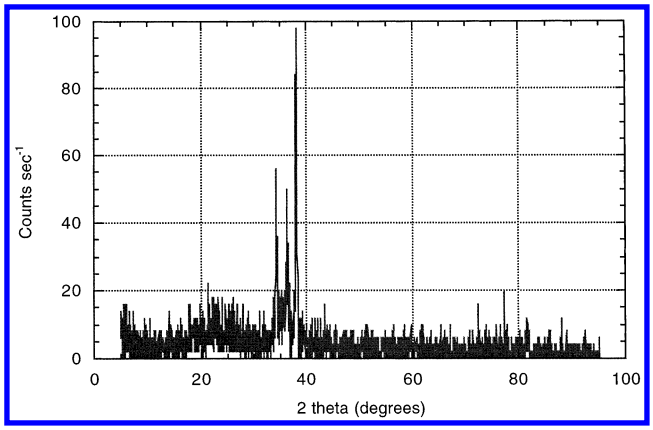

Figure 7. $\theta-2\theta$ scan of 8 monolayers of $(Bu_2N\varphi V)_2BuPy^+I^-$, on a "Au|Ti|glass" substrate shows a Cu Kα Au (111) peak at 38.12°, a Cu Kβ Au (111) peak at 34.22°, and a shifted Ti peak at 36.26°.

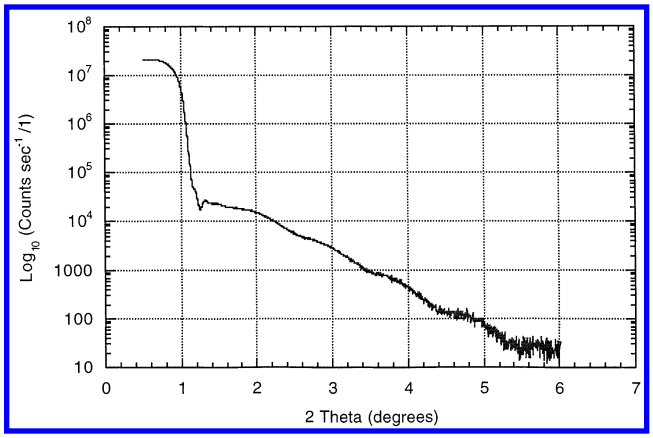

Figure 8. X-ray reflectivity of 8 monolayers of $(Bu_2N\varphi V)_2BuPy^+I^-$, on a "Au|Ti|glass" substrate (50 nm Au, 20 nm Ti) shows Kiessig fringes from the gold.

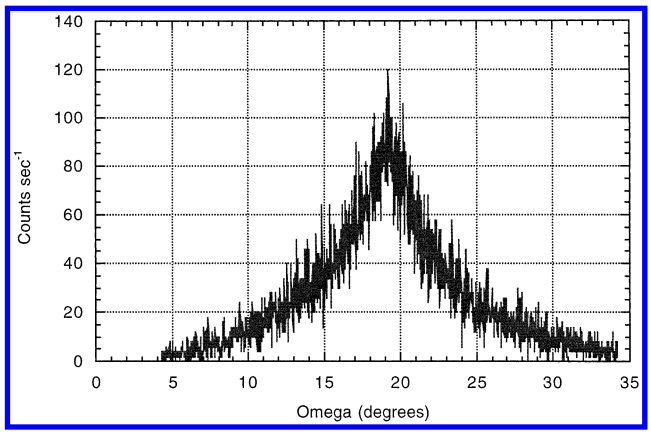

Figure 9. X-ray (Cu Kα) rocking curve of 8 monolayers of $(Bu_2N\varphi V)_2BuPy^+I^-$, on a "Au|Ti|glass" substrate for the Au (111) peak shows a wide distribution of orientations of the Au (111) planes.

493 nm; therefore, the components should increase with decreasing wavelength.

X-ray diffraction of a multilayer (8 monolayers) was chosen to determine the thickness per monolayer. A large-angle scan is shown in Figure 7, while the region of low angles was also scanned, but with larger integration time and higher resolution, as shown in Figure 8. The large-angle scan of Figure 7 shows that the gold surface is only Au(111), but the rocking curve of Figure 9 shows that there is a large distribution of Au(111) plane orientations in the sample. Further analysis of the low-angle data (using a background correction, an initial box model fit,

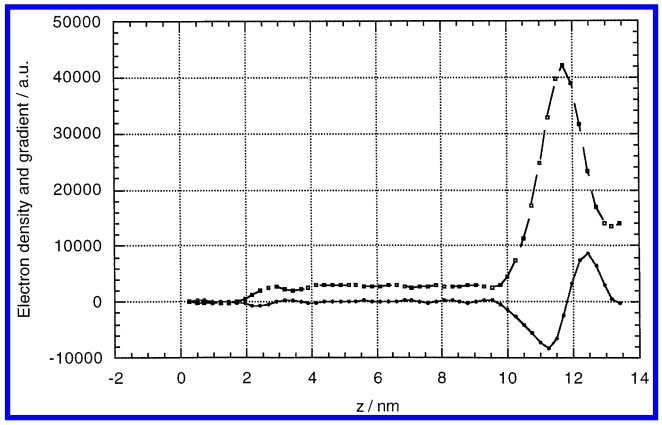

Figure 10. Electron density (top) and gradient (bottom) from X-ray diffraction of 8 LB monolayers of $(Bu_2N\varphi V)_2BuPy^+I^-$, on a "Au|Ti|glass" substrate showing air−LB film interface (approximately 2 nm) and LB film−Au interface (approximately 11 nm).

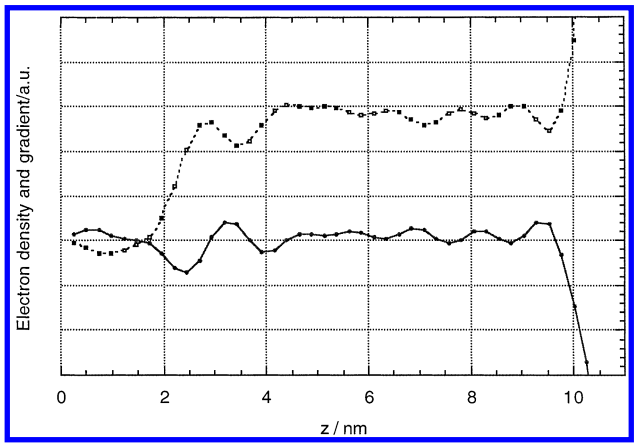

Figure 11. Electron density (top) and gradient (bottom) from X-ray diffraction of 8 LB films of $(Bu_2N\varphi V)_2BuPy^+I^-$ on Au substrate, enlarged to show the LB film region. It is clear that there are at least 6 LB monolayers present from $z = 1.5$ to $z = 9.5$, and that the spacing between layers is approximately 1.3 nm.

and subsequent refinement using the measured data),[15,16] yielded the electron density and its gradient as a function of distance from the surface (Figure 10 and Figure 11). This analysis clearly shows the monolayer structure, though only 6 monolayers seem to be present, with a spacing of approximately 1.3 nm between monolayers.

Second-Harmonic Generation. The monolayer exhibits a strong second-harmonic intensity corresponding to an effective second-order susceptibility of 50 pm V^{-1} at normal incidence and to an optimum of 150 pm V^{-1} at 45° for $\lambda = 1064$ nm (Nd:YAG, p-polarized). There is a weak polarization dependence, $I^{2\omega}(p \rightarrow p)/I^{2\omega}(s \rightarrow p) \approx 2$, and the variation of the second-harmonic intensity with the angle of incidence of the laser beam, relative to the film, shows a broad maximum at 45 ± 10° (Figure 12). Although subject to large error, the angle at maximum intensity should approximate the angle required to rotate a limb of the chevron (an intramolecular charge-transfer axis) perpendicular to the beam. We note that the optimum susceptibility is comparable with those obtained for the extensively studied hemicyanine dyes[17] and even higher than many. It confirms that the structure is noncentrosymmetric and suggests that the molecules are optimally aligned.

Rectification. Thirty-two MOM assemblies were measured, each with top pad area = 0.3 mm^2; of these, 3 were short circuits, mainly due to the inability to control the thickness of the top gold electrode or due to imperfections in the LB film.

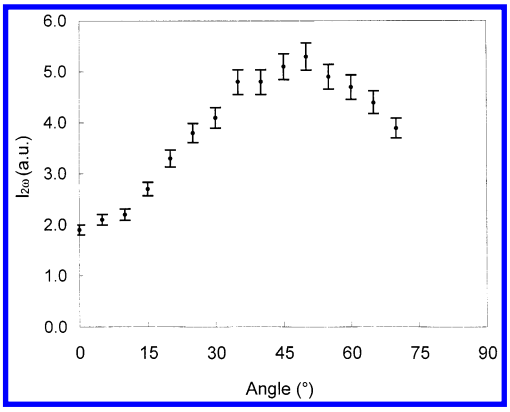

Figure 12. Variation of the square root of the second-harmonic intensity with the incident angle of the laser beam ($\lambda = 1064$ nm) for an LB monolayer of $(Bu_2N\varphi V)_2BuPy^+I^-$.

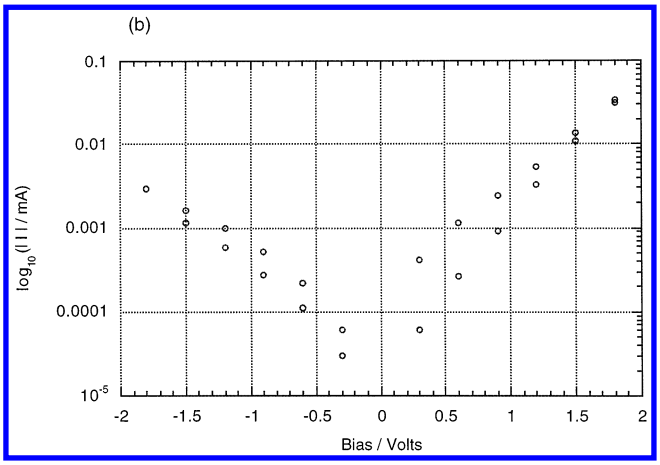

Figure 13. $I-V$ characteristics of a monolayer of $(Bu_2N\varphi V)_2BuPy^+I^-$ between gold electrodes. (a) I versus V plot, showing decreasing rectification after each cycle (highest RR = 12 at $V_0 = 1.8$ V; for scans 1−6, RR = 12, 7, 5, 4, 3, 3, respectively. (b) A log(|I|) vs V plot, for the first scan only (RR = 12).

When the top gold electrode is too thin, there is uneven coverage of the surface, because gold tends to form microscopic gold spheres, which unevenly coat the surface, allowing electrical shorts to occur to the bottom electrode. The 29 remaining MOM assemblies had DC resistances of 1 to 60 kΩ, and of these, 24 had rectifying behavior, and 5 had symmetrical $I-V$ curves. In contrast to a previous study,[6,18] no reverse rectification was seen for any pad.

The average RR at $V_o = 1.5$ V is 8.4, with a standard deviation of 16, due to the high RR of several pads (60, 48, 11). If we exclude these three RR values from the statistics, the average RR goes down to 2.5, with a standard deviation of less than one, at 1.25 V. At $V_o = 1.8$ V, the average RR increases to above 4 at ±1.8 V, which corresponds to a field of approximately 900 MV m^{-1} and a current density of 10 to 1000 mA cm^{-2}. Repeated measurement of the same MOM leads to a decreased RR, so that the IV asymmetry disappears after 5 to 15 cycles. Figure 13 shows a typical $I-V$ curve for a monolayer of $(Bu_2N\varphi V)_2BuPy^+I^-$ between two gold electrodes. Above a threshold voltage (V_t), the monolayer shows higher currents at positive bias than for the corresponding negative bias. V_t varies from junction to junction in the range 0.5 to 1.0 V. Under positive bias, the easy-current direction, the top electrode is positive and electrons flow from the bottom electrode to the top electrode. The pyridinium iodide is believed to be on the bottom gold electrode, with the iodide closest to the gold surface.

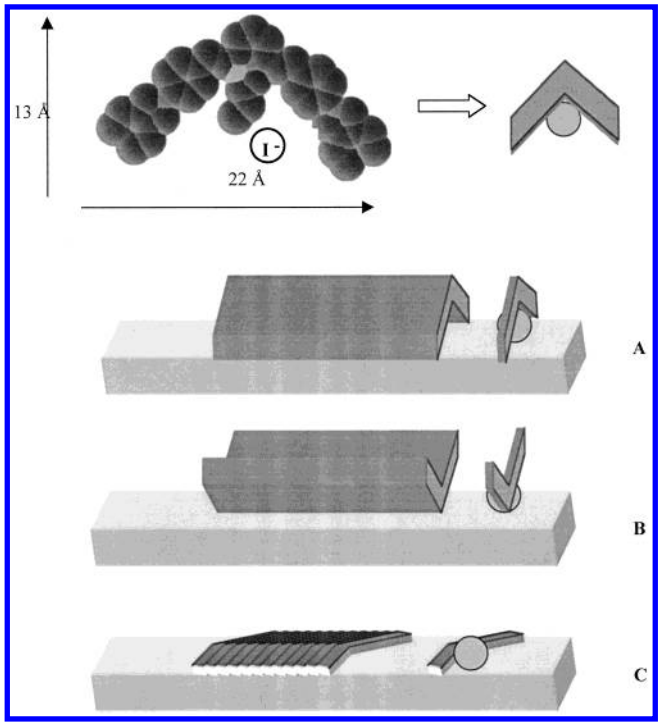

Figure 14. Three possible arrangements of individual molecules of $(Bu_2N\varphi V)_2BuPy^+I^-$ on the air−water interface during the LB transfer, taking into account the area per molecule at transfer $A_t = 90$ Å^2 at the transfer pressure of 22 mN m^{-1} and the X-ray thickness of 13 Å. The fully extended trans-configuration has a molecular length = 22 Å, height = 13 Å, and width = 3.5 Å.

Discussion

The hypsochromic shift observed in polar solvents (λ_{max} = 519 nm in chloroform, (λ_{max} = 508 nm in acetone, and (λ_{max} = 505 nm in acetonitrile) can be attributed to a back electron transfer from the iodide anion to the pyridinium cation, in analogy to previous work.[12,13,19] One may wonder whether enough iodide ion is actually present in the LB monolayer, since for a similar pyridinium bromide, no Br signal was detected by X-ray photoelectron spectroscopy.[20] Therefore, finding only one-third as much signal from the iodine as expected for a 1:1 complex, $(Bu_2N\varphi V)_2BuPy^+I^-$ may be due to insufficient XPS sensitivity to halogens.

If one estimates the molecular length as 22 Å and the molecular width as 8 Å, one obtains a calculated area of 175 Å^2, close to A_o. The molecule, $(Bu_2N\varphi V)_2-BuPy^+I^-$, is drawn in Figure 14 in a chevron configuration, which is an approximation of the lowest-energy configuration found by using the PM3 algorithm (Figure 2). The molecule is almost certainly in a chevron or V configuration, with the center of the chevron being the pyridinium moiety, and the arms of the chevron are the dibutylaminophenylvinyl moiety. If we take into account the area per molecule at transfer $A_t = 90$ Å^2 (95 ± 5 Å^2 from QCM) at the transfer pressure of 22 mN m^{-1}, and the calculated extended length of the molecule (22 Å), the calculated height (13 Å), and the calculated width (3.5 Å), we can draw three schematics of the possible arrangement of the molecules on the air−water interface during the LB film transfer. These three arrangements are shown in Figure 14. The iodide diameter is 4.1 Å, which has significance for the film thickness. Iodide (and other halides) are known to chemisorb strongly onto gold.[21] This assumption is used in all three models (A, B, C) of Figure 14. There is evidence to suggest that there is significant electron transfer from the iodide ion to the pyridinium ring both in the literature,[12,13,19] and in the UV−vis spectrum of Figure 4.

The X-ray thickness data are more reliable than ellipsometry data, since ellipsometry fits are known to have false convergence; this leaves the thickness of the monolayer at approximately 13 Å, which fits with the idea of a compressed monolayer (100 Å^2 at transfer). This would push the chevron arms either down or up, which leads us to believe that either model A or B is correct. There should be sufficient distance in the vertical direction to account for the arms (10 Å) plus the iodide (4 Å), which gives a reasonable picture of the surface of the monolayer, and corresponds well to the measured data. Since the iodide is assumed on the gold surface, then either model A or B of Figure 14 will fit the mechanism of electron transfer from the iodide to the pyridinium ring.

The important experimental finding is that electrons flow more easily, at $V > V_t$, from the bottom Au electrode, through the monolayer, to the top Au pad; given that the monolayer was transferred atop the bottom Au electrode on the upstroke, the iodide ion (if present) is probably closest to the bottom electrode, at some unknown but relatively small distance from the pyridinium ion. If the dominant mechanism were electron transfer from the dibutylaminophenyl ring to the pyridinium ion, then enhanced electron motion would occur in the direction opposite to what is observed. Therefore it is likely that, at positive bias, electron transfer or charge transfer (CT) occurs from the iodide ion (or whatever anion is present) to the pyridinium ring; this CT is well-known in this type of molecule, allowing the iodide to donate an electron to the pyridinium functional group.[12,13,19]

Another point should be considered: a recent theoretical study has shown that *IV* asymmetries can occur whenever the relevant groups between which push−pull effects are registered is placed asymmetrically in the gap.[22] And, indeed, the iodide−pyridinium ion pair is probably asymmetrically placed within the gap.

If we take the work function of Au as 5.3 V, then enhanced current flows in the "Au|DBAP−HT−BPy^+I^-|Au" sandwich at 5.3 − (0.5 to 1.0) = 4.3 to 4.8 V below the vacuum level. Of the calculated MO levels (10.4 eV for HOMO, 4.6 eV for LUMO) for an ion very similar to DBAP−HT−BPy^+, only the LUMO seems to be well placed in energy, relative to observation. This situation was also seen for hexadecylquinolinium tricyanoquinodimethanide,[6] for which the rectification is assumed to be due to intramolecular electron transfer.[6,7]

In conclusion, the asymmetric *IV* curves reported here seem to be due to enhanced back electron transfer from iodide to pyridinium ion. This is an organic analogue of a Schottky barrier rectifier.[23]

Acknowledgment. We are grateful to Dr. Paul L. Evans for collecting the X-ray reflectivity data. The work at the University of Alabama was supported by NSF-DMR-FRG-00-95215 "Oligomolecular Nanodevices".

References and Notes

(1) Aviram, A.; Ratner, M. A. *Chem. Phys. Lett.* **1974**, *29*, 277−283.
(2) Metzger, R. M.; Panetta, C. A. *New J. Chem.* **1991**, *15*, 209−221.
(3) Metzger, R. M. In *Molecular and Biomolecular Electronics*; Birge, R. R., Ed.; ACS Adv. In Chem. Ser. 240; American Chemical Society: Washington, DC, 1994; pp 81−129.
(4) Ashwell, G. J.; Sambles, J. R.; Martin, A. S.; Parker, W. G.; Szablewski, M. *J. Chem. Soc. Chem. Commun.* **1990**, 1374−1376.
(5) Martin, A. S.; Sambles, J. R.; Ashwell, G. J. *Phys. Rev. Lett.* **1993**, *70*, 218−221.
(6) Metzger, R. M.; Chen, B.; Hopfner, U.; Lakshmikantham, M. V.; Vuillaume, D.; Kawai, T.; Wu, X.; Tachibana, H.; Hughes, T. V.; Sakurai, H.; Baldwin, J. W.; Hosch, C.; Cava, M. P.; Brehmer, L.; Ashwell, G. J. *J. Am. Chem. Soc.* **1997**, *119*, 10455−10466.
(7) Metzger, R. M. *Acc. Chem. Res.* **1999**, *32*, 950−957.

(8) Ashwell, G. J.; Gandolfo, D. S. *J. Mater. Chem.* **2001**, *11*, 246−248; *J. Mater. Chem.* **2002**, *12*, 411−415.
(9) Kretschmann, E. *Z. Phys.* **1971**, *313*, 241.
(10) Okazaki, N.; Sambles, J. R. In *International Symposium on Organic Molecular Electronics*; Nagoya, Japan, May 18, 2000; pp 66−67.
(11) Metzger, R. M.; Xu, T.; Peterson, I. R. *J. Phys. Chem. B* **2001**, *105*, 7280−7290.
(12) Verhoeven, J. W.; Dirkx, I. P.; De Boer, Th. J. *Tetrahedron* **1969**, *25*, 3395−3405.
(13) Kosower, E. M.; Skorcz, J. A. *J. Am. Chem. Soc.* **1960**, *82*, 2195−2203.
(14) Sauerbrey, G. *Z. Phys.* **1959**, *155*, 206−222.
(15) Metzger, R. M.; Baldwin, J. W.; Shumate, W. J.; Peterson, I. R.; Mani, P.; Mankey, G. J.; Morris, T.; Szulczewski, G. J.; Bosi, S.; Prato, M.; Commito, A.; Rubin, Y. Manuscript in preparation.
(16) Forkan, M. G.; Peterson, I. R.; Miller, L. S.; Parry, D. A.; Walton, D. J. *Langmuir* **2000**, *16*, 8057−8062.
(17) Ashwell, G. J. *J. Mater. Chem.* **1991**, *9*, 1991−2003.
(18) Vuillaume, D.; Chen, B.; Metzger, R. M. *Langmuir* **1999**, *15*, 4011−4017.
(19) Reichardt, C. *Solvents and Solvent Effects in Organic Chemistry*, 2nd ed.; VCH: Weinheim, Germany, 1988; pp 292−293.
(20) Ashwell, G. J.; Hamilton, R.; Wood, B. J.; Gentle, I. R.; Zhou, D. *J. Mater. Chem.* **2001**, *11*, 2966−2970 (December 2001).
(21) Chen, A. C.; Shi, Z. C.; Bizzotto, D.; Lipkowski, J.; Pettinger, B.; Bilger, C. *J. Electroanal. Chem.* **1999**, *467*, 342−353.
(22) Krzeminski, C.; Delerue, C.; Allan, G.; Vuillaume, D.; Metzger, R. M. *Phys. Rev. B* **2001**, *64*, #085405.
(23) Geddes, N. J.; Sambles, J. R.; Jarvis, D. J.; Parker, W. G.; Sandman, D. J. *J. Appl. Phys.* **1992**, *71*, 756−768.